

LASER INTERFEROMETER GRAVITATIONAL WAVE OBSERVATORY

– LIGO –

CALIFORNIA INSTITUTE OF TECHNOLOGY
MASSACHUSETTS INSTITUTE OF TECHNOLOGY

LIGO-T010064-00-R

5/31/2001

**A Study of Gravitational Waves
and the response of Advanced LIGO
as top-level parameters are varied**

Lisa Goggin, Alan Weinstein

California Institute of Technology
LIGO Project – MS 51-33
Pasadena, CA 91125
Phone (626)395-2129
Fax (626)304-9834
E-mail: info@ligo.caltech.edu

Massachusetts Institute of Technology
LIGO Project – MS 20B-145
Cambridge, MA 01239
Phone (617)253-4824
Fax (617)253-7014
E-mail: info@ligo.mit.edu

WWW: <http://www.ligo.caltech.edu>

A Study of Gravitational Waves

Lisa M. Goggin, University College Cork

Supervisors:

Professor Alan Weinstein, California Institute of Technology

Professor Niall O Murchadha, University College Cork

April, 2001

Abstract

Astrophysicists predict that inspiraling neutron star binary systems in the final seconds before merger are likely to be the first sources to be seen by the LIGO detector, as they fall within the LIGO frequency band. Gravitational waves emitted by such systems will have a 'chirp' waveform. By Fourier transforming this signal and comparing it to the expected level of noise in the interferometer, we can estimate the signal to noise ratio, (S/N), for such a signal emitted by a binary at a specified distance; or, for a fixed S/N threshold the distances at which such sources are just detectable. The Advanced LIGO detector is limited by seismic noise at low frequencies, thermal noise at intermediate frequencies and shot noise at high frequencies. We vary some of the parameters determining each of the noise levels for different detector configurations: seismic wall cut-off frequency; test mass mirror Q and signal mirror transmittance and tune phase. We evaluate the binary inspiral benchmark (detectable distance) for each configuration as a function of the parameters governing these noise sources. This is used to optimise the Advanced LIGO detector response, and aids in making detector cost / performance trade-offs.

1. Introduction

Gravitational waves are ripples in space-time due to the acceleration of masses, in much the same way that electromagnetic waves are emitted by accelerating charges. The existence of such entities was first postulated by Einstein in his General Theory of Relativity in 1916, (as described in [1]). Gravitational waves have never been experimentally observed but their existence has been indirectly verified by Hulse and Taylor [2]. Gravitational waves carry with them information about their origins and fundamental properties such as speed and polarisation, or equivalently, the mass and spin of the associated quantum mechanical particle, the graviton. Their detection would provide us with information about strong-field gravity, and about the astrophysical sources such as binary inspirals, pulsars and supernovas as well as relic gravitational waves from the 'Big Bang'. There have been attempts in the past to detect gravitational waves using various methods, most notably resonant bar detectors, however, none of these yielded significant results. At the present time the gravitational wave community is focusing its efforts on interferometric methods of detecting gravitational waves: LIGO in the US; TAMA in Japan; VIRGO in Italy; GEO600 in Germany and ACIGA in western Australia.

In this project we study the waveform of gravitational waves emitted by an inspiraling binary neutron star system. We apply this to the Advanced LIGO detector and investigate some of the factors limiting its sensitivity over the relevant bandwidth.

2. Gravitational Waves

Gravitational waves expected from anticipated astrophysical sources can be divided into four classes: the 'chirp' signal from the inspiral of compact binaries; periodic waves from pulsars; impulsive waveforms from supernova bursts and stochastic background from the Big Bang or from distant faint sources. In the last few seconds before merger, compact binaries emit gravitational waves in the LIGO band. Astrophysicists [1] predict that these are likely to be the first known sources to be detected by LIGO. In this project we concentrate on neutron star binary systems, seconds before the two stars coalesce.

The gravitational wave field produces a dimensionless strain $\Delta x/x$ of space and its strength is characterised by the gravitational field amplitude, h . As the wave propagates from its source, h falls off as $1/r$, i.e. the inverse of the distance travelled from the source. The expected amplitude from astrophysical sources at the earth is of the order of 10^{-21} or less. Thus, the effect of a gravitational wave on two test masses a distance 1m apart is to change their separation by an amount $\Delta x = 10^{-21}$ m. Given that this variation is so small, the task of detecting gravitational waves against background noise is very difficult.

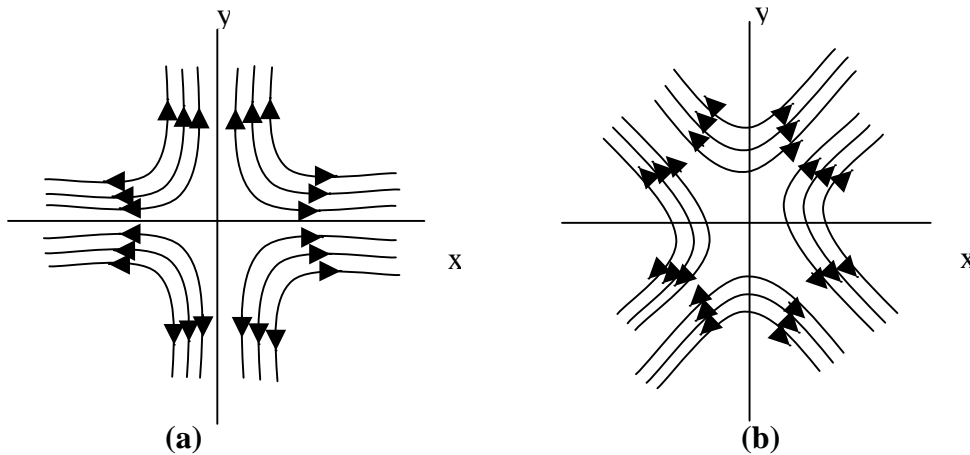


Fig. 1. Gravitational wave force fields; (a) 'plus' polarisation (b) 'cross' polarisation

Gravitational waves may be resolved into two linearly polarised components each with its own time-evolving waveform. These produce force fields with the orientation of a plus sign and a cross sign denoted by h_+ and h_x respectively (Fig. 1). The effect of a gravitational wave of polarisation h_+ on a ring of test masses is to deform the ring into an ellipse that pulsates in and out in the x and y directions. The h_x polarisation has a similar effect, but at an angle at 45° to the x and y axes (Fig. 2).

The spin of the zero mass particle associated with the quantum mechanical description of a wave is defined as $360^\circ/\theta$, where θ is the angle of rotation about which the wave is invariant. As can be seen from Fig. 2, for a gravitational wave $\theta = 180^\circ$, which yields the value 2 as the spin of the graviton. Analogously for electromagnetic waves, the photon has spin 1.

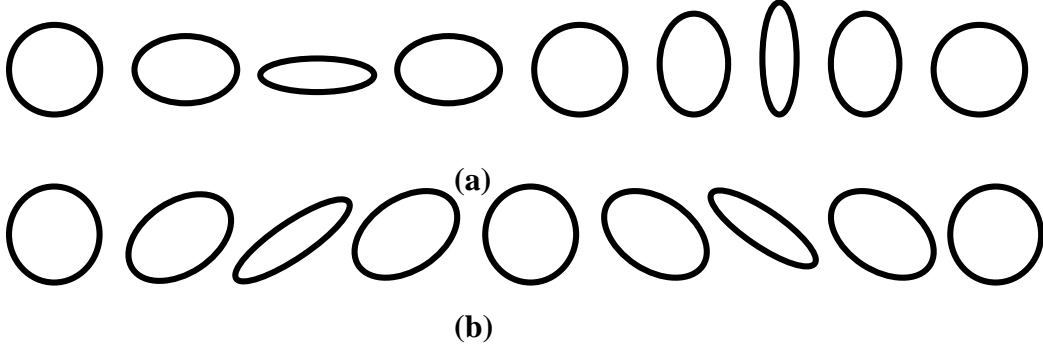


Fig.2. Effect of (a) h_+ and (b) h_x on ring of test masses

3. Chirp Waveform

The frequencies of the chirp waveform are in the audio band, and they sweep from low to high frequency resembling the chirp of a bird. The chirp waveform is one of the few waveforms from an astrophysical source that can be calculated with confidence. Thus, it is used as a 'standard candle' to evaluate the performance of a detector.

Consider two masses M_1 and M_2 , a distance a apart, orbiting each other under the force of gravity. As the two bodies spiral together, they emit periodic gravitational waves and consequently the evolution of the orbital radius is given by [1]

$$a = a_0 \left(1 - \frac{t}{\tau_0} \right)^{\frac{1}{4}}, \quad (i)$$

where a_0 is the radius of the orbit at $t=0$ and the spiral time, τ_0 , is given by [1]

$$\tau_0 = \frac{5}{256} \frac{a_0^4}{\mu M^2} \frac{c^5}{G^3}, \quad (ii)$$

where M is the total mass of the system and μ , the reduced mass. Therefore our system of neutron binaries with $M_1 = M_2 = 1.4M_{sol}$, (where M_{sol} is the solar mass) initially a distance 10^5 km apart, will coalesce in approximately 0.37s. The frequency, f , of the waves, (which is twice the orbital frequency), is [3]

$$f = \frac{1}{\pi} \left[\frac{5}{256} \frac{1}{\mu M^{\frac{2}{3}}} \frac{1}{(\tau_0 - t)} \frac{c^5}{G^{\frac{5}{3}}} \right]^{\frac{3}{8}}. \quad (iii)$$

The two polarization amplitudes of gravitational waves at a distance D from the source are given in the Newtonian regime by [3]

$$h_+ = 2(1 + \cos^2 i)(\mu / D)(\pi Mf)^{\frac{2}{3}} \cos(2\pi ft) \frac{G^{\frac{5}{3}}}{c^4},$$

$$h_x = \pm 4 \cos i (\mu / D)(\pi Mf)^{\frac{2}{3}} \sin(2\pi ft) \frac{G^{\frac{5}{3}}}{c^4}, \quad (\text{iv})$$

where i is the binary inclination angle, such that $i = 90^0$ corresponds to the system visible edge-on. Thus, if the binary is a distance of 100Mpc away from the Earth, then the amplitude of the gravitational wave reaching the earth as the stars coalesce will have a magnitude of 10^{-22} , and h_+ (or h_x) has a chirp waveform as shown in Fig. 3. As can be seen the amplitude varies slowly until the very final stages where it blows up. It is here that the post-Newtonian approximation breaks down and the waveform is unknown. At this point for a neutron star binary system tidal forces rip the stars apart and so detection of the waveform from such a system would provide us with information about its nuclear equation of state.

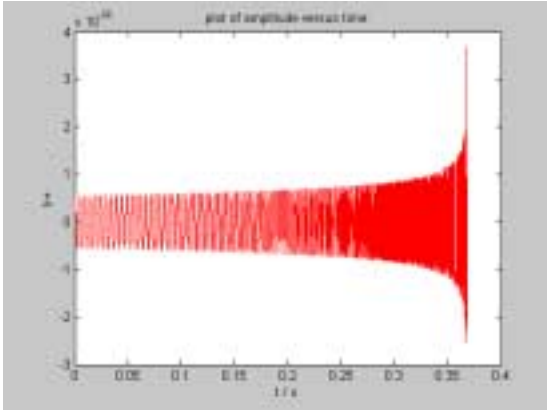


Fig. 3. 'Chirp' signal from the inspiral of binary star system 100Mpc away.

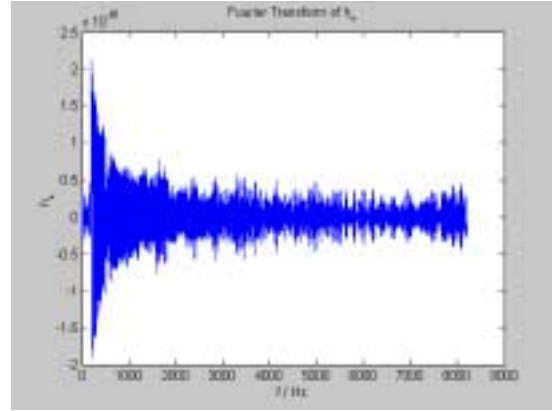


Fig.4. Fast Fourier Transform of h_+ .

The performance of a gravitational wave detector is characterised by the noise level in the frequency domain and thus we want to study the chirp waveform in the frequency domain. This is achieved in *Matlab* by taking the Fast Fourier Transform of the chirp waveform (iv), the result of which is shown in fig. 4.

We can now compare the chirp waveform to the noise by evaluating the signal to noise ratio, S/N , and thus evaluate the sensitivity of the detector as a function of source distance. The Fast Fourier Transform, (fft) of the plus and cross polarisations (iv) were combined according to equation (v) to give the averaged characteristic gravitational wave amplitude [3]

$$h = \sqrt{|h_+ \sim|^2 + |h_x \sim|^2}, \quad (\text{v})$$

shown in fig. 5. This shows that the power decreases at higher frequencies, as the time spent at anyone finite frequency band gets smaller as the frequency increases.

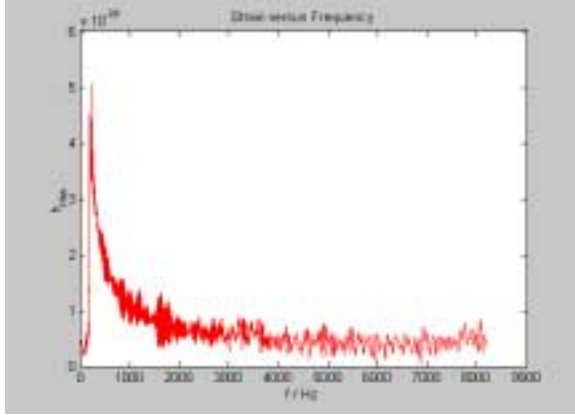


Fig.5. Absolute value of Fast-Fourier Transformed amplitudes

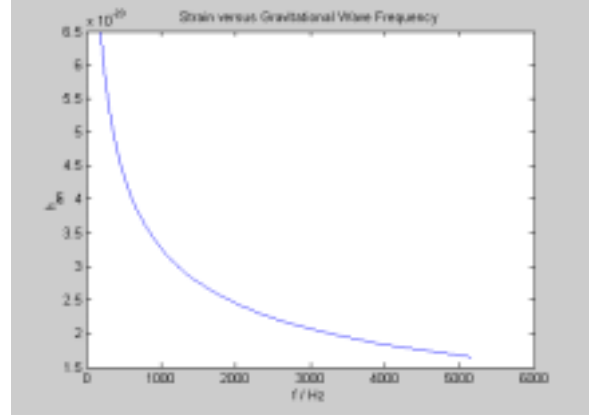


Fig. 6. Plot of strain as given by equation (vi)

The analytic form of equation (v), formed by Fourier transforming equations (iv), squaring and averaging over the inclination angle is given by the following equation [3] and shown in fig. 6.

$$h = \sqrt{\langle |h_+|^2 + |h_x|^2 \rangle} = \left(\frac{\pi}{12} \left(\frac{\mu}{D} \right)^2 \frac{M^3}{\mu} \frac{1}{(\pi M f)^{7/3}} \frac{G^5}{c^3} \right)^{1/2}. \quad (\text{vi})$$

We plot in fig. 7 both of the above signals, on a log log scale

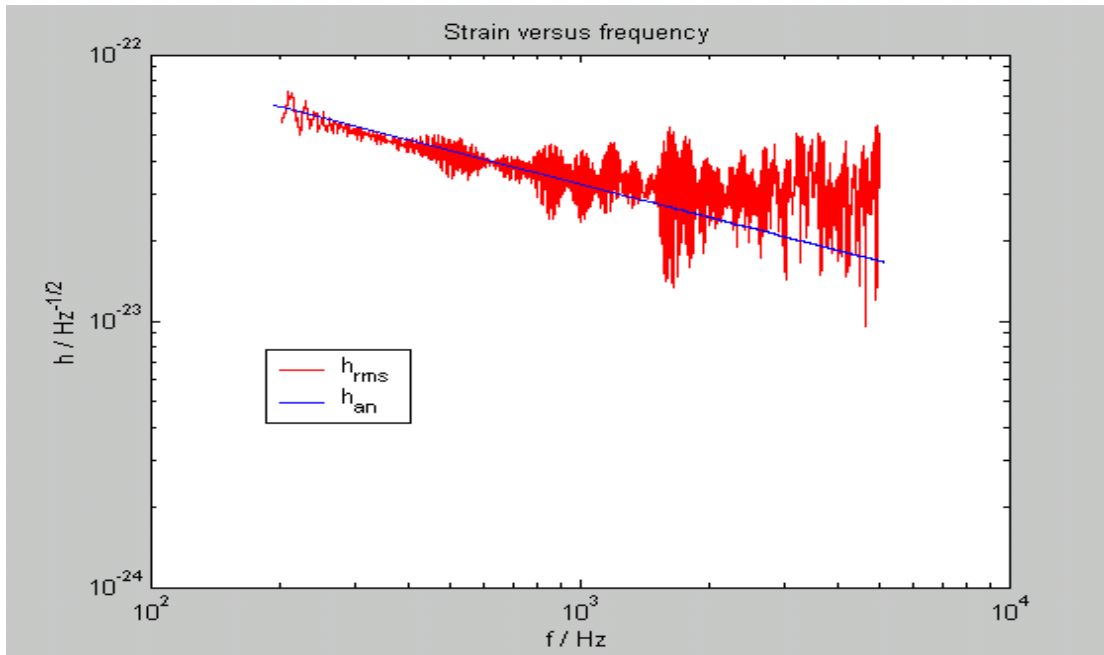


Fig. 7. Log-log plot of strain in units of 1/rtHz, versus frequency

When a scaling factor (whose relevance is not yet quite understood) was applied to equation (v) the two curves agreed quite well.

4. Gravitational Wave Interferometers

Ground based gravitational wave detectors are capable of detecting signals of frequency $>10\text{Hz}$. Seismic and other earth-based environmental noise sources overcome any expected astrophysical signal at lower frequencies; thus for lower frequencies, space based interferometers are required. The Laser Interferometer Gravitational-wave Observatory, LIGO, is limited by fundamental noise sources: seismic noise at low frequencies; thermal noise at intermediate frequencies and shot noise at high frequencies. Seismic noise, examples of which are ground vibrations due to man-made sources such as traffic and wind forces coupled to the ground by trees, is transmitted to the test masses through their suspensions. The intermediate frequency noise is due to off-resonance, thermally induced vibrations of the test masses and their suspensions. Shot noise is due to the randomness in the number of photons arriving at the photo-detector, for small signals. Radiation pressure noise is the fluctuations in test mass position caused by photons bouncing off of the mirrored surfaces.

The 'signal to noise' ratio, S/N depends on the level of noise in the interferometer. To optimise the interferometer we first have to evaluate the S/N for the gravitational wave sources that we wish to detect. This allows us to make trade-offs in the performance versus cost and the ability to suppress detector noise. To help do this the *Matlab* program, *bench*, was written, [4], to calculate different figures of merit for use in detector design. Bench takes as an argument an interferometer configuration, specified in terms of its optical properties, substrate properties and suspension properties. It evaluates the level of fundamental noise expected from such an interferometer (fig.8), and then calculates an 'effective distance' R_0 , at which an optimally oriented source can be detected with a S/N of 8. The event rate goes like volume and thus is proportional to R_0^3 .

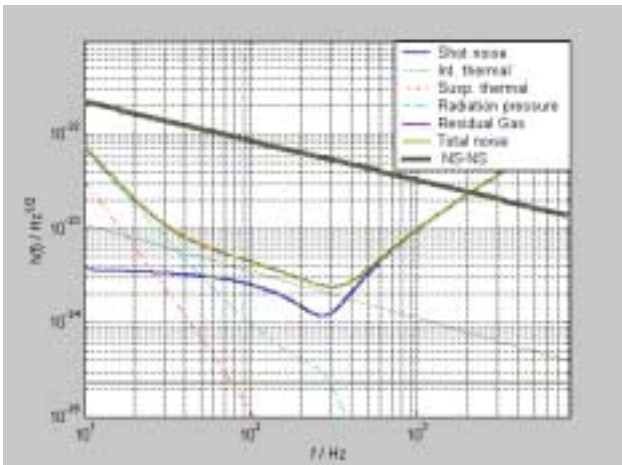


Fig. 8. Log-log plot of the interferometer noise and neutron binary signal

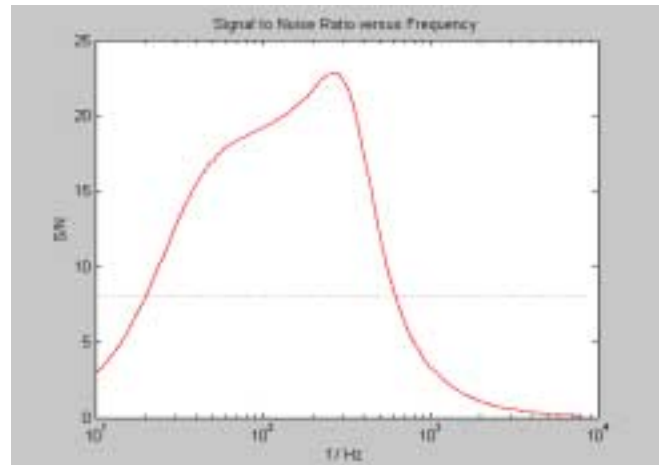


Fig. 9. Signal to noise ratio for neutron star binary at 100Mpc

Using as our model an Advanced LIGO configuration of an interferometer with silica test masses and a seismic wall at 10Hz, we obtain a binary inspiral benchmark value of 168 Mpc . (Other parameters determining R_0 which will be varied later (stated here for comparative purposes) are test mass mirror $Q = 3 \times 10^7$, signal mirror transmittance, $T = 0.12$ and tune phase, $\phi = 0.2$.) . Fig. 8 displays the individual noise curves, the total noise and the binary signal. However, we are only interested in regions where $S/N > 8$, i.e. between the reasonably broad band of frequencies - 21 and 600 Hz, as shown in fig. 9.

5. Noise Sources

5.1 Seismic Noise

By modifying the noise constraints we can decide how best to maximise our sensitivity to binary inspirals. First we deal with the seismic noise. For current and planned seismic isolation systems, this is a sharply falling function of frequency,

$$n \propto \frac{1}{f^{12.5}}, \quad (\text{vi})$$

and thus behaves like a 'wall' at low frequencies, (~ 10 Hz). Using advanced seismic isolation technologies, the position of the wall can be moved to lower frequencies, but with considerable cost and effort. As can be seen from Fig.10 in varying the seismic wall, f_s , from 4 to 40Hz, R_0 goes from 168 Mpc to 148 Mpc. R_0 falls increasingly fast between 4 and 25 Hz and then decreases approximately linearly.

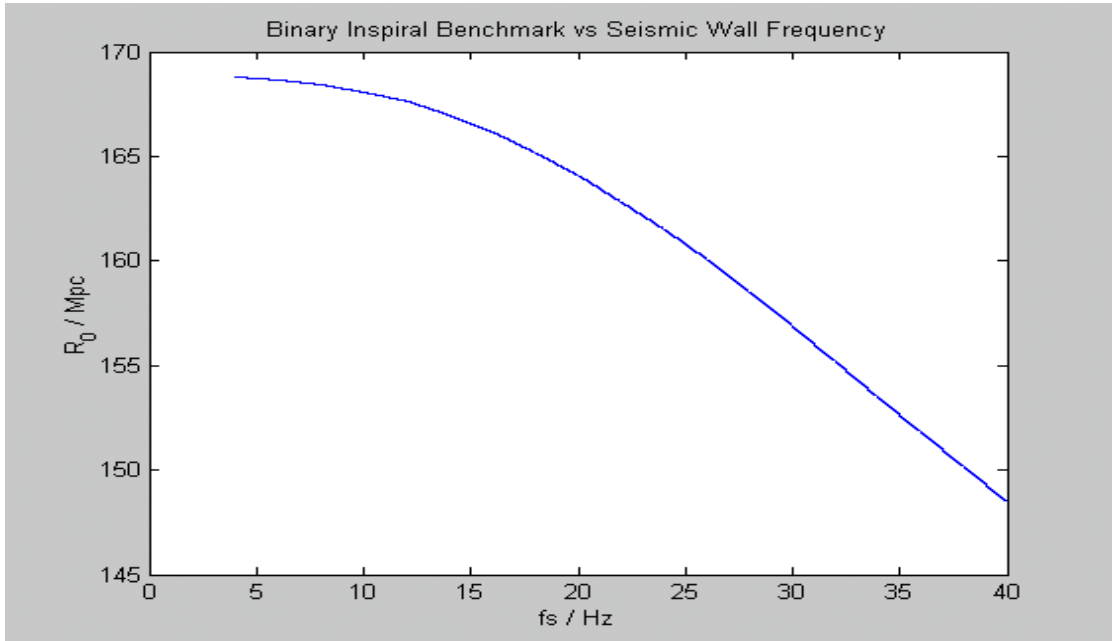


Fig. 10 Binary inspiral benchmark versus seismic wall frequency

5.2 Thermal Noise

In an interferometric gravitational wave detector, the most important point at which thermal noise will appear is at the front surface of a test mass. The thermal noise power spectrum is dominated by internal modes of the test mass itself and vibrational modes of the pendulum suspension wires. The suspension modes depend on properties of the suspension wires as well as the number of wires and the mirror mass. The contribution of the thermal noise to the strain sensitivity, h , has a frequency dependence proportional to $1/f^5$, and thus the strain noise in $1/\text{Hz}^{1/2}$ goes as $1/f^{2.5}$. The internal modes, whose noise contribution is inversely proportional to frequency, consists of a thermoelastic and a normal mode contribution. The former depends on properties of the test mass material such as thermal conductivity, thermal expansion and heat capacity as well as properties of the laser and interferometer such as beam radius and cavity length. The normal mode contribution (at frequencies far from the normal mode frequencies) has an inverse dependence on the mirrors quality (Q) factor. (The mechanical Q -factor is the ratio of the resonant frequency to the full-width at half maximum of the resonance peak). This is a consequence of the Fluctuation-Dissipation theorem. Thus in order to reduce the noise we choose materials which maximise Q and place the resonances either below ($\sim 10\text{Hz}$) or above ($\sim 10\text{kHz}$) the frequencies of interest. However, achieving high Q mirrors is a difficult challenge in materials science. Q 's in the range of 10^7 are achievable using fused silica mirrors and one may achieve higher Q 's, in excess of 10^8 , using crystalline sapphire.

To study the effect of thermal noise on R_0 we varied the Q of the test mass mirrors from 10^6 to 10^9 , (the nominal value is taken to be 3×10^7). This analysis resulted in a variation of R_0 from 47 to 257 Mpc as shown in fig. 11. As can be seen, the rate of increase in R_0 is greatest between Q values of 10^7 and 10^8 . The rate of growth beyond 10^8 is considerably less.

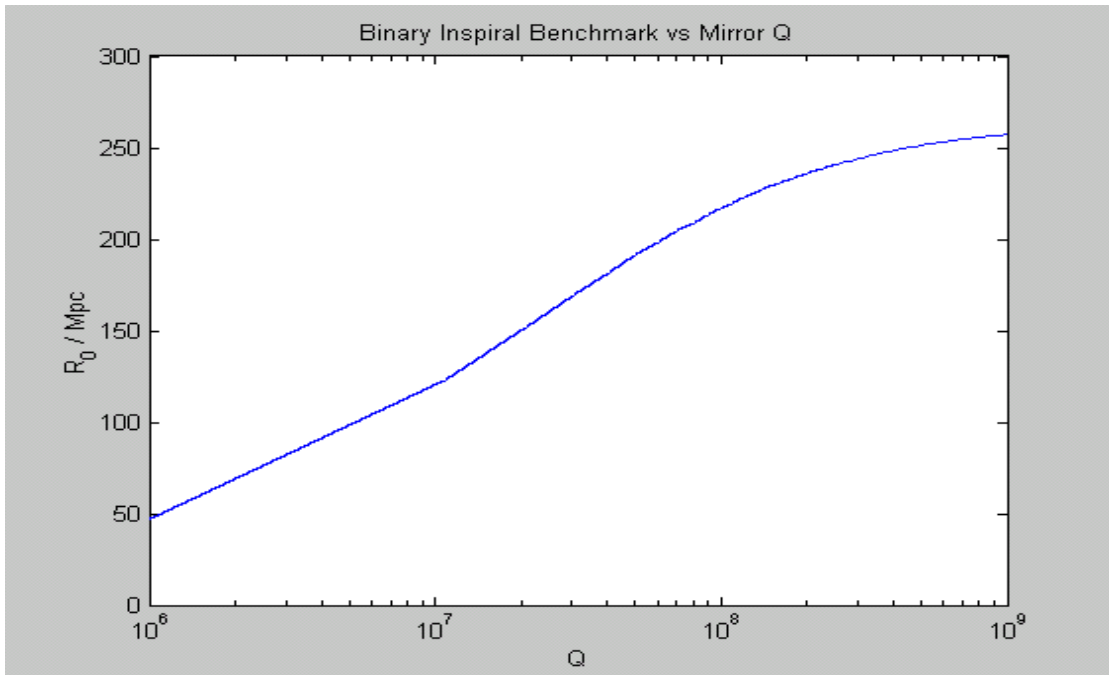


Fig. 11. Binary inspiral benchmark versus mirror Q

5.3 Shot Noise & Radiation Pressure Noise

Shot noise is the statistical fluctuation in the number of photons arriving at the photodetector, making the inferred position of the test masses uncertain. The already well-developed methods for reducing shot noise are the use of high powered lasers and power recycling. An increase in laser power by a factor x increases the sensitivity by $x^{1/2}$ and reduces the shot noise contribution to the strain by $1/x^{1/2}$. The sensitivity of the interferometer in response to a gravitational wave can be further enhanced by manipulating the shot noise response of the gravitational wave signal imprinted on the laser light exiting the asymmetric port of the Michelson interferometer, using a signal recycling mirror. This can be achieved by making sub-wavelength position changes in the signal recycling mirror position (in the asymmetric port) and changing the transmissivity of the signal recycling mirror. The contribution of the shot noise to the strain sensitivity h has the following frequency dependence

$$n \propto \left(\frac{f}{\sin(af)} \right)^2, \quad (\text{viii})$$

where a is a constant. The noise also depends on the phase shift, ϕ , of the light and transmittance, T , of the signal mirror in the dark port such that

$$n \propto \frac{e^\phi}{T^2}. \quad (\text{ix})$$

Radiation pressure, which tends to displace the mirrors from their resonant position resulting in the detuning of the cavity has a $1/f^2$ frequency dependence and is related to the signal mirror transmittance and phase shift by

$$n \propto \frac{T^2}{e^\phi}. \quad (\text{x})$$

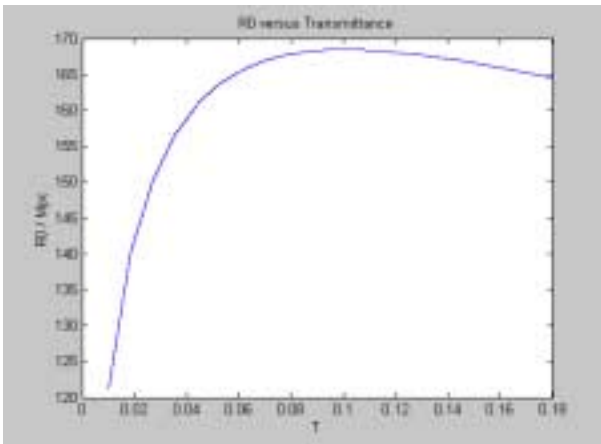


Fig. 12 Binary inspiral benchmark versus signal mirror transmittance.

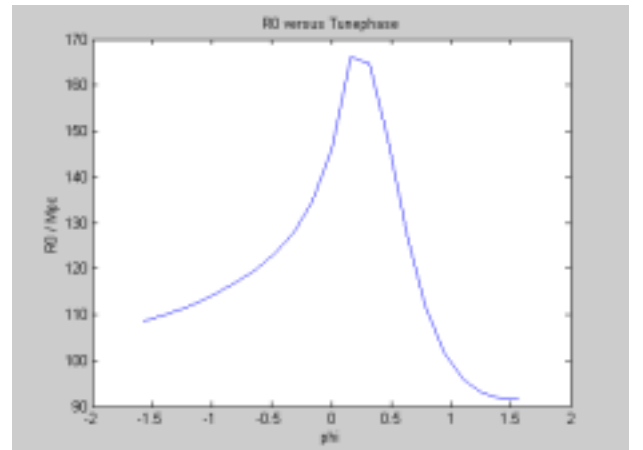


Fig. 13. Binary inspiral benchmark versus signal mirror tune phase

We study the dependence of the effective distance R_0 on the shot noise and radiation pressure noise response by changing the position, x , of the signal mirror relative to its

position when the carrier laser light is resonant in the signal recycling cavity, (or, equivalently, the ‘tune phase’ of the laser light in the cavity, $\phi = 2x / \pi\lambda$, where $\lambda = 1 \mu\text{m}$, is the wavelength of the laser light) and reflectivity of the signal mirror in the dark port. Fig 12 displays the dependence of R_0 on the transmittance for tune phase fixed at 0.2. R_0 increases sharply over a short range of T before reaching a maximum at 168 Mpc corresponding to a transmittance of 0.1 and then falls off gradually. The variation of the binary inspiral benchmark with tune phase, keeping the transmittance fixed at 0.21, is displayed in fig. 13. R_0 peaks at a value of $\phi = 0.1$. When both transmittance and tune phase are varied over intervals of 0 to 0.18 and $-\pi/2$ to $\pi/2$ respectively, R_0 has the form shown in Fig 14.

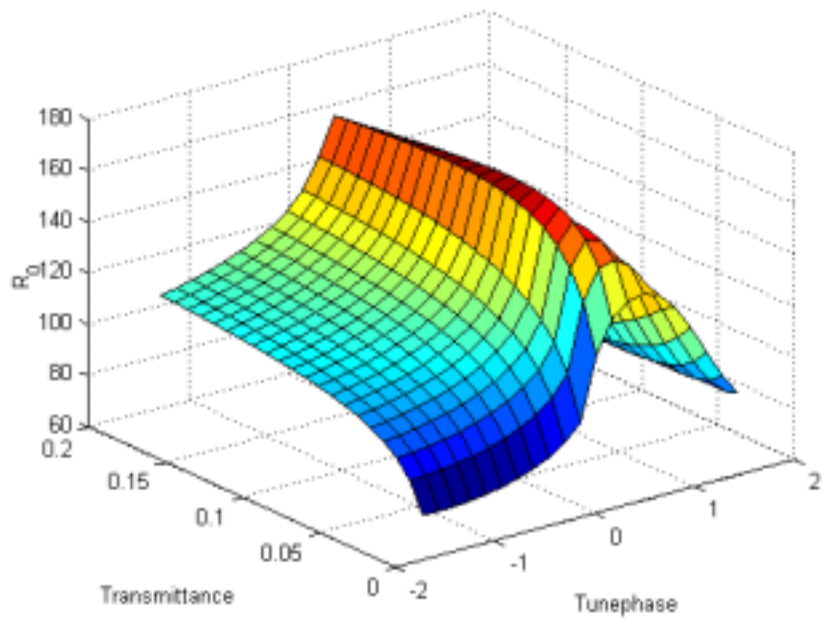


Fig. 14. Binary inspiral benchmark versus transmittance and tune phase

To see the effect of these parameters on the shot noise and radiation pressure noise we pick representative points from the 3-D plot in figure 15.

(a) $T = 0.85$ $\phi = -\pi/2$ $R_0 = 119 \text{ Mpc}$

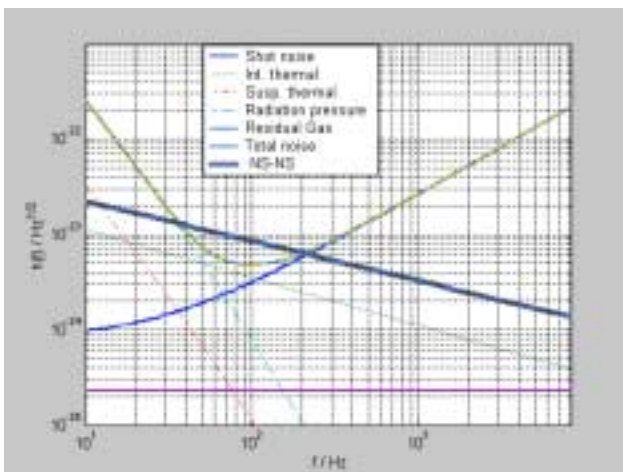


Fig 15

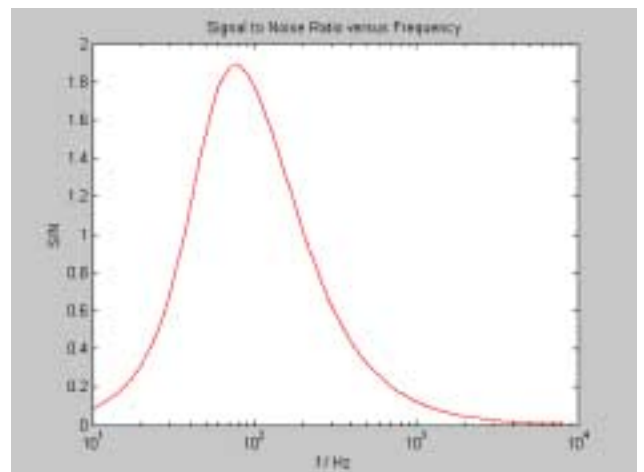


Fig 16

(b) $T = 0.22$ $\phi = 0$ $R_0 = 150$ Mpc

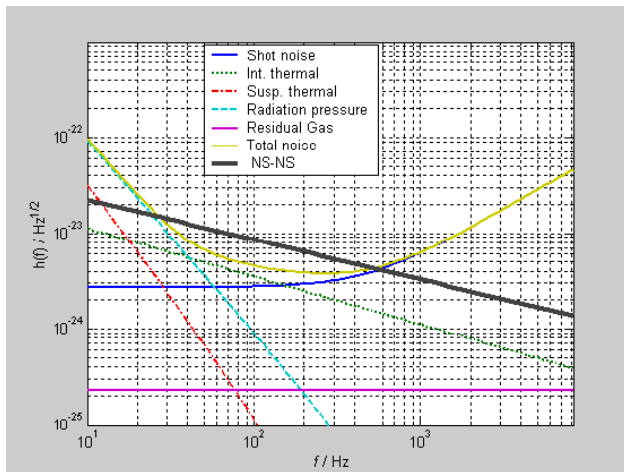


Fig. 17

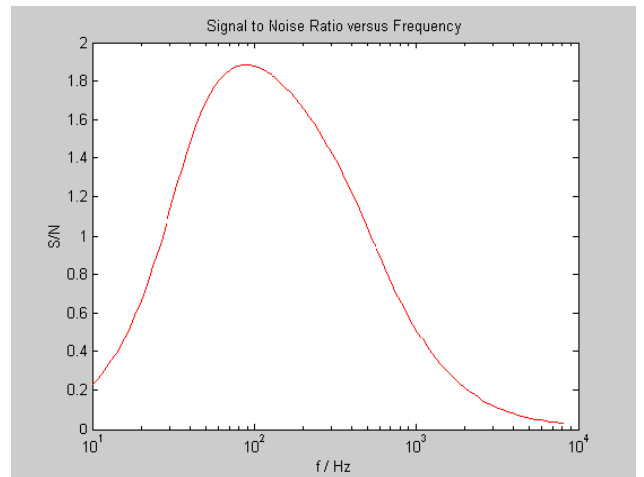


Fig 18

(c) $T = 0.2$ $\phi = \pi/2$ $R_0 = 95$ Mpc

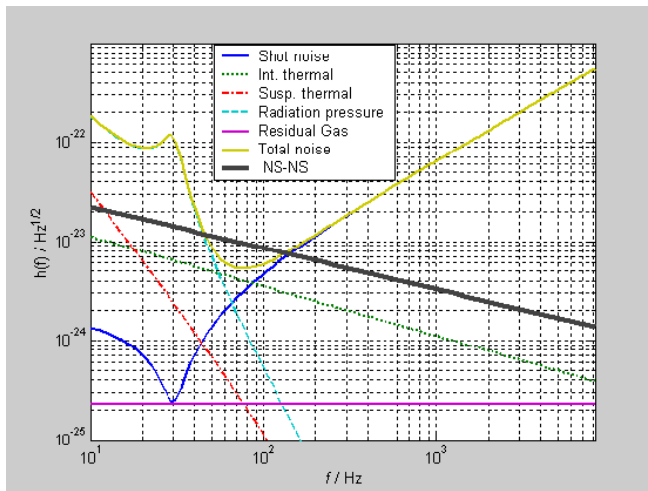


Fig 19

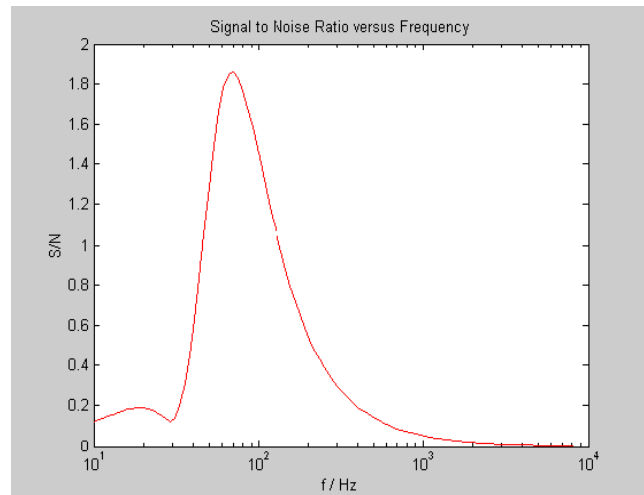


Fig 20

(d) $T = 0.02$ $\phi = -\pi/2$ $R_0 = 86$ Mpc

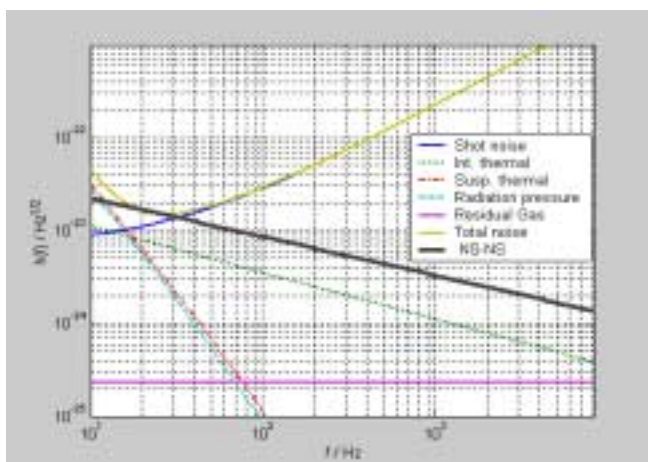


Fig. 21

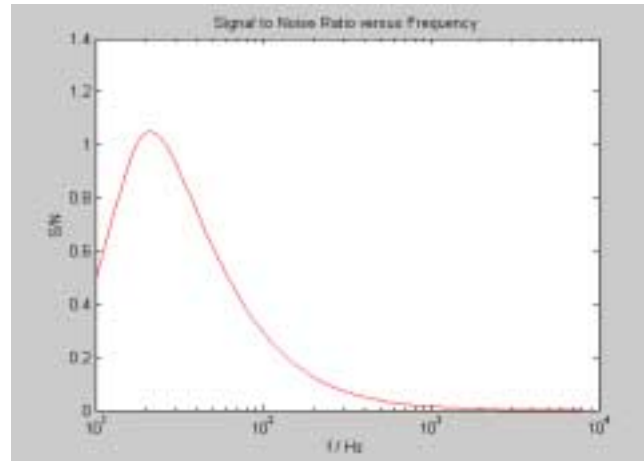


Fig. 22

(e) $T = 0.11$ $\phi = \pi/2$ $R_0 = 91$ Mpc

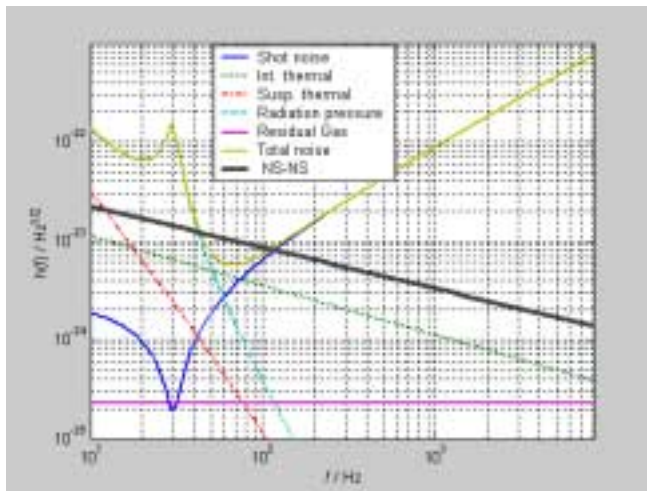


Fig. 23

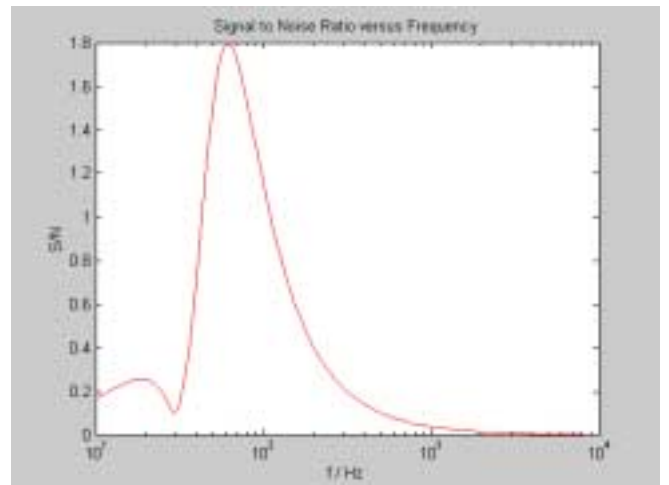


Fig. 24

(f) $T = 0.06$ $\phi = 0.1$ $R_0 = 154$ Mpc

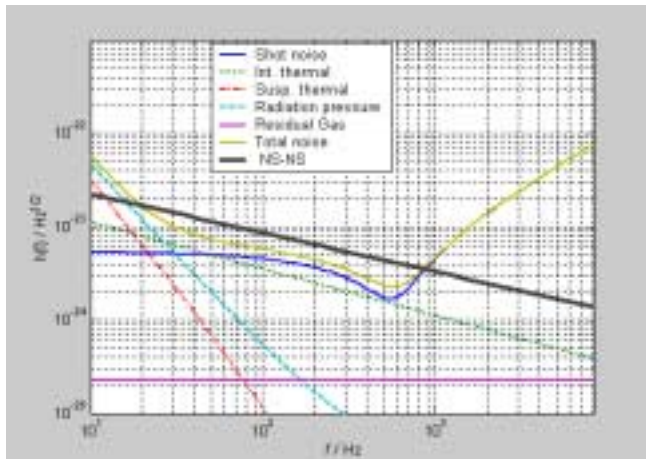


Fig. 25

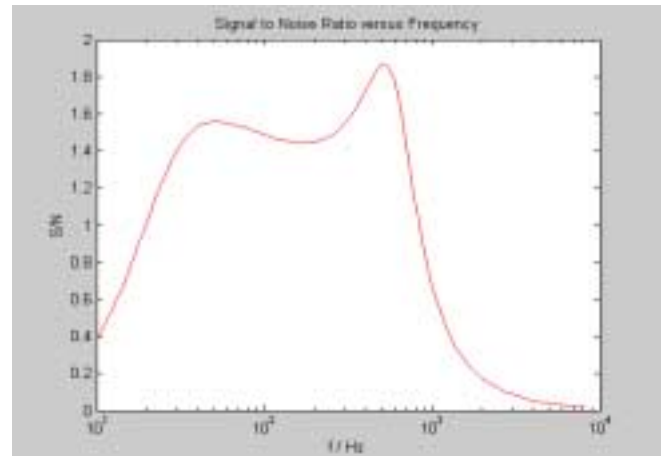


Fig. 26

(g) $T = 0.1$ $\phi = 0.1$ $R_0 = 160$ Mpc

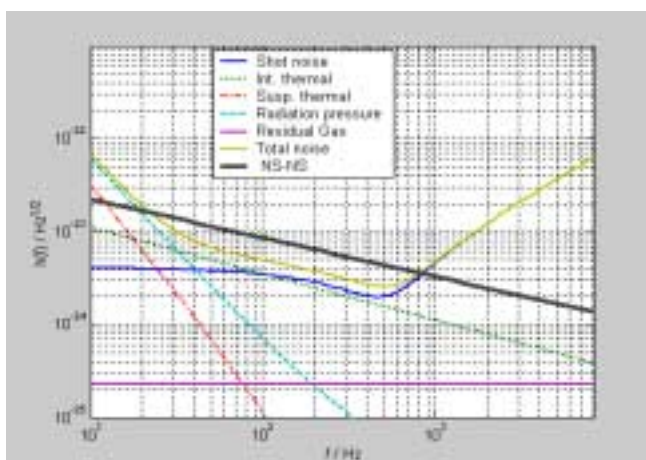


Fig. 27

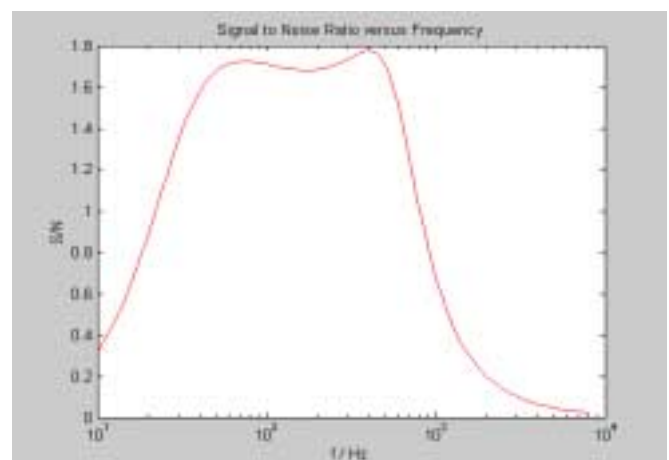


Fig. 28

(a) With a tune-phase of $-\pi/2$ the transmittance curve peaked at 0.85. With these values the radiation pressure is high at low frequencies but falls off quickly. The shot noise is low at low frequencies but increases quickly, dominating the total noise curve from approximately 12 Hz as shown in fig 15. As a result the plot of signal to noise ratio versus frequency, fig. 16, displays a high but narrow peak around 100 Hz. The binary inspiral benchmark for this configuration is 119 Mpc.

(b) The optimum transmittance for a tune phase of 0 was 0.22. As can be seen from fig. 17 the shot noise curve was approximately constant at low frequencies, increasing slowly at higher frequencies. Compared with the previous case the radiation pressure noise line did not decrease as sharply. R_0 here was found to be 150 Mpc, indicating that these parameters are more favourable. This is also clear from fig. 18 as the S/N curve is much broader.

(c) With a tune phase of $\pi/2$ and transmittance of 0.2 the binary inspiral benchmark returned was 95 Mpc. The reason behind this low result can be seen from fig 19. The radiation pressure curve begins to decrease from an initially high value of h , but then increases before decreasing rapidly again. More importantly however, the shot noise begins at a low value of h and decreases to a minimum before increasing sharply, thus yielding a very narrow frequency band with significant S/N , fig. 20.

(d) For comparison we next take two points from fig 14 which gave particularly low values of R_0 : $T=0.02$, $\phi=-\pi/2$ and $T=0.11$, $\phi=\pi/2$. For the first of these, the shot noise dominates over practically the whole frequency range, fig 21, and the signal is eclipsed above 100 Hz, as shown in fig. 22. R_0 in this case is 86 Mpc.

(e) The second of these 'bad' points gave a slightly higher R_0 of 91 Mpc. The noise curve, fig. 23, is similar to that (c) discussed above, except that the radiation pressure noise curve now intersects the shot noise curve at slightly lower frequency.

(f) The values of transmittance and tune phase which are currently considered favourable are 0.06 and 0.1 respectively. This combination gave a binary inspiral benchmark of 154 Mpc. As can be seen from fig. 25, the shot noise curve stays close to the signal line up to approximately 250 Hz. This is reflected in fig. 26 as the S/N is significant over a broad range of frequencies.

(g) Finally taking the peak values of the transmittance and tune phase curves from figs. 12 and 13, 0.1 and 0.1 respectively, R_0 was 160 Mpc. In this instance, the shot noise curve fig. 27, varies less than in the previous case. The S/N curve, fig. 28 is similar to that of fig. 26, but constant over a broader band.

6. Conclusion

With the configuration currently described by the 'bench' program, (also described in section 4) LIGO will detect binary inspirals with $S/N > 8$ up to a distance of 168 Mpc away. This is in the frequency bandwidth approximately between 21 and 600 Hz.

In fig. 10 we saw that R_0 varies very little below 15 Hz, so perhaps the cost in moving the seismic wall below this frequency would not merit the results. Also, looking at all of the noise curves, the radiation pressure curve limits the low frequencies and did not change significantly with any of the changes to T and ϕ .

On increasing the mirror Q from 10^7 by a factor of 10, R_0 almost doubles, and, as the event rate is proportional to R_0^3 , this increases by a factor of 8. Thus, it appears that achieving a Q of 10^8 would considerably increase LIGO's scope. As with the seismic noise, a technical evaluation would decide if the increase in R_0 that a higher mirror Q factor yields would be feasible.

Given the broad-band nature of the inspiral signal, and the presence of fundamental thermal noise at intermediate frequencies, optimal sensitivity is attained when the signal recycling mirror transmission T and tune produce a shot noise curve which 'hugs' the thermal noise curve, as closely as possible, out to the highest frequencies. The narrow-banding, (eg. figs 19 and 23) capabilities of signal recycling do not pay off in the presence of this level of thermal noise. However, such narrow-banding will be useful when searching for inherently narrow-band sources (such as pulsars) at higher frequencies.

Combining the 'optimum' value for each parameter, i.e. $f_s = 10$ Hz, $Q = 10^8$, $T = 0.1$, $\phi = 0.1$ gave a binary inspiral benchmark of 191 Mpc, figs 29, 30. If f_s was changed to 15 Hz and each of the other parameters remained unchanged, R_0 decreases to a value of 190 Mpc, while seismic wall frequency of 20 Hz yields an R_0 of 187 Mpc, which does not appear to be a significant loss of information.

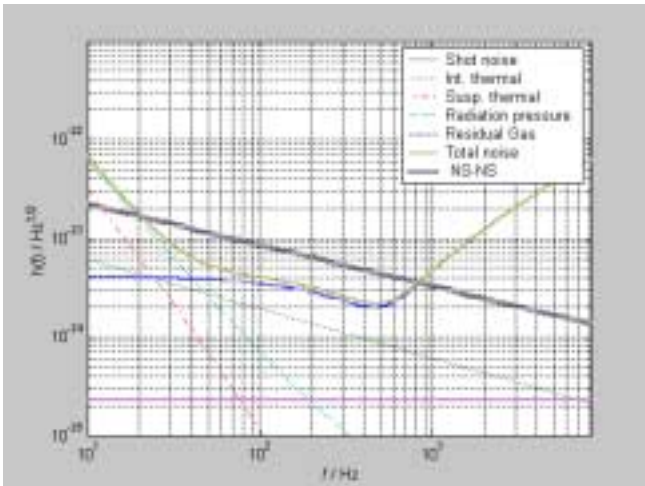


Fig. 29

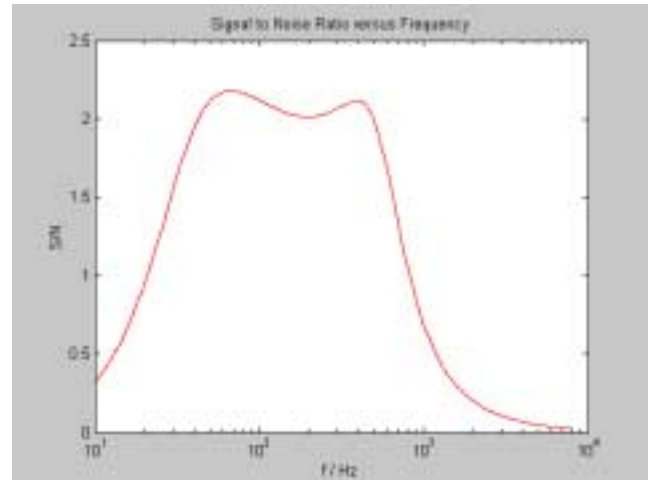


Fig. 30

7. Acknowledgements

I wish to thank Alan Weinstein for once more giving me the opportunity to work on the LIGO project and providing me with direction and motivation for the duration of the project and in writing this paper. Thanks to Niall O' Murchadha for his supervision and for offering much helpful advice in dealing with the more complex issues encountered in the project. Many thanks also to Dr. Jim Grannell and Mr. Paul Keegan for the provision of the necessary software and computer facilities.

8. References:

- [1] Misner C. W., Thorne K. S., Wheeler J. A., '*Gravitation*', 1970
- [2] Taylor J. H., Weisberg J. M., *Astrophys. J.* **345**, 434 (1989)
- [3] Thorne K. S., '*300 Years of Gravitation*', Ch.9; 1987
- [4] Finn L.S., *IFOModel.m, bench.m* <http://gravity.phys.psu.edu/~lsf/Benchmarks>
- [5] Abramovici A. et al, *Science*, vol. **256**, 325 (1992)
- [6] Finn L. S., *Phys Rev D*, vol. **53**, 2878, (1996)
- [7] Grishchuk L. P. et al, astro-ph/0008481 vol. **3**, (2001)
- [8] Thorne K. S., <http://www.lsc-group.phys.uwm.edu/lscasis/docs/KipCutoff.ps>

Appendix 1

Summary of results for the binary inspiral benchmark, R_0 , returned with varying the following parameter: seismic wall frequency, f_s ; test mass Q-factor, Q ; signal mirror transmittance, T and tune phase, ϕ .

f_s / Hz	$Q \times 10^7$	T	ϕ	R_0 / Mpc
10	3	0.12	0.2	168
10	3	0.85	-1.57	119
10	3	0.22	0	150
10	3	0.2	1.57	95
10	3	0.02	-1.57	86
10	3	0.11	1.57	91
10	3	0.06	0.1	154
10	3	0.1	0.1	160
10	10	0.06	0.1	179
10	10	0.1	0.1	191
15	10	0.1	0.1	190
20	10	0.1	0.1	187